Local Free Volume and Structure of Polymer Gel Electrolytes on the Basis of Alternating Copolymers

A. Reiche,*,† G. Dlubek,‡,§ A. Weinkauf,† B. Sandner,† H. M. Fretwell,§ A. A. Alam,§ G. Fleischer,|| F. Rittig,|| J. Kärger,|| and W. Meyer⊥

Institut für Technische und Makromolekulare Chemie, Martin-Luther-Universität Halle-Wittenberg, Geusaer Strasse, D-06217 Merseburg, Germany, ITA Institut für innovative Technologien GmbH, Köthen, Aussenstelle Halle, Wiesenring 4, D-06210 Lieskau (Halle/S.), Germany, H. H.Wills Physics Laboratory, University of Bristol, Tyndal Avenue, Bristol BS8 1TL, U.K., Fakultät für Physik und Geowissenschaften, Institut für Experimentelle Physik, Universität Leipzig, Linnéstrasse 5, D-04103 Leipzig, Germany, and Max-Planck-Institut für Polymerforschung, Ackermannweg, 10, D-55128 Mainz, Germany

Received: December 9, 1999; In Final Form: March 1, 2000

The relationship between the structure of the polymer and the charge carrier mobility and the ionic conductivity has been studied for a new class of gel electrolytes on the basis of alternating copolymers. These gel electrolytes were prepared by photopolymerization of maleic anhydride and oligo(ethylene glycol)$_4$ divinyl ether in the presence of various oligo(ethylene glycol)$_n$ dimethyl ethers with molar masses between 134 and 2000 g/mol, and $LiCF_3SO_3$. Thermal properties of the materials were studied by differential scanning calorimetry and dynamic mechanical analysis, which additionally gives structural information. Changes in the free volume as a function of the content of the plasticizer and the salt were studied by positron annihilation lifetime (PAL) spectroscopy. The self-diffusivity of charge carriers and plasticizer in the gel electrolytes was investigated by pulsed field gradient NMR. The ionic conductivity and its pressure dependence were determined by the impedance technique. The gel electrolytes studied are heterogeneous materials composed of a highly cross-linked polymer network ($M_c \approx 600$ g/mol) with a $T_g \approx 100$ °C and of a plasticizer−salt solution with a $T_g \approx -70$ °C. Hence, two hole size distributions were measured by PAL spectroscopy around 0.26 and 0.34 nm related to the network and the liquid phase, respectively. The activation volume V^* calculated from the pressure dependence of the ionic conductivity was $V^* = 22.7$ cm^3/mol. It is concluded that the charge carrier transport occurs in the liquid phase of the gel electrolytes. However, the network is too dense to provide sufficient distribution and mobility of the plasticizer−salt solution. Self-diffusivity and conductivity of the gel electrolytes studied are not related according to the Nernst−Einstein equation. The ortho-positronium (o-Ps) lifetime τ_3 and its intensity I_3 in the gel were found to be changed if salts were added to the gel. The o-Ps lifetime is discussed in terms of o-Ps bubbles in the plasticizer−salt solution. The o-Ps intensity I_3, which decreases with the salt concentration, mirrors inhibition reactions of the o-Ps formation attributed to the anions of the salt.

1. Introduction

Transport processes in polymers such as viscous flow and the self-diffusion can be described in terms of the free volume by the well-known Dolittle[1] and Cohen−Turnbull[2] models. Self-diffusivity and ionic conductivity are related by the Nernst−Einstein relationship. Therefore, the ionic conductivity of polymer electrolytes should also depend on the free volume. However, the study of the free volume is rather complicated. Electrochromic, photochromic, and fluorescent probes are described in the literature. Positron annihilation lifetime spectroscopy (PAL spectroscopy) is a further well-established and very sensitive technique for probing subnanometer-sized local free volumes in solids and liquids.[3−6] Briefly described, a fraction of positrons injected in molecular materials such as polymers, will form a bound state called a positronium (Ps).[7] The Ps appears either as a para-positronium (p-Ps, singlet spin state) or as an ortho-positronium (o-Ps, triplet spin state), with a relative abundance of 1:3. In a vacuum, an o-Ps has a relatively long lifetime of 142 ns. When injected into matter, the Ps may collide with atoms or molecules and the positron of the Ps may annihilate with an electron other than its bound partner and with opposite spin (pick-off annihilation). The result is a sharply reduced o-Ps lifetime depending on the collision frequency. Given a sufficiently large concentration of holes (local free volumes) in the sample, the Ps density is largely restricted to these open volumes, and the o-Ps pick-off lifetimes, which are typically in the nanosecond range, can be evaluated to estimate the size of the holes.[8−10] Typical o-Ps lifetimes in glassy polymers have values from ∼1600 ps (epoxy resins)[32] to ∼2000 ps (polycarbonates),[23] while in rubbery polymers lifetimes of 2500 ps (polybutadiene)[33] and larger values may be observed.

First studies of the free volume in relationship to the ionic conductivity indicate that the temperature dependence of the ionic conductivity can be explained by free volume changes. Wang et al.[11,12] found a correlation of the fractional free volume

† Martin-Luther-Universität Halle-Wittenberg.
‡ ITA Institut für innovative Technologien GmbH.
§ University of Bristol.
|| Universität Leipzig.
⊥ Max-Planck-Institut für Polymerforschung.

10.1021/jp994331d CCC: $19.00
Published on Web 06/16/2000

and the conductivity of polyether urethane−$LiClO_4$ complexes for temperatures above the glass transition of the polymer. However, the mobility of cations and anions in polymer electrolytes depends also on the interaction of the polymer and the charge carriers. Besides changes in the charge carrier mobility, the ionic conductivity is furthermore influenced by the number of charge carriers with dependence on the ionic association. Therefore, changes of the ionic conductivity with dependence on the salt content and the role of the plasticizer could not fully be understood by PAL spectroscopic measurements only.[11−15] For example, Forsyth et al.[13,14] found that the addition of propylene carbonate or olig(ethylene glycol)$_4$ dimethyl ether ((EG)$_4$DME) to polyether urethane networks results in a similar increase in the free volume; however, the ionic conductivity was effected in a different manner.

In the present work, we used PAL spectroscopy to investigate the effect of (EG)$_{11}$DME as a plasticizer and various conducting salts on the free volume in a network of poly(maleic anhydride-*alt*-oligo(ethylene glycol)$_4$ divinyl ether) (poly(MAN-*alt*-(EG)$_4$DVE)).

The applicability of alternating copolymers obtainable by copolymerization of the electron acceptor maleic anhydride (MAN) and the electron donor oligo(ethylene glycol)$_4$ divinyl ether ((EG)$_4$DVE) as a matrix for polymer electrolytes was recently described.[16−18] Gel electrolytes on the basis of these monomers can be prepared by in situ photopolymerization of the comonomer mixture without any photoinitiator in the presence of a lithium salt and of various plasticizers. Compared to gel electrolytes on the basis of poly((ethylene glycol)$_n$ dimethacrylate) (poly((EG)$_n$DMA), higher cationic transference numbers, an improved electrochemical stability, and enhanced mechanical strength of the films can be achieved.[17−19] However, the ionic conductivity of poly(MAN-*alt*-(EG)$_4$DVE)-based gel electrolytes is distinctly lower.[17] Higher conductivities can be reached by use of terpolymers of MAN and (EG)$_4$DVE with butylvinyl ether or ethoxy tri(ethylene glycol) methacrylate, which have a distinctly lower network density than the former.[17,18]

From this point of view, a more comprehensive investigation of the polymer and the gel structure in relation to their electrochemical properties was of interest. In addition to the study of these gel electrolytes by PAL spectroscopy, the thermal properties of the materials were investigated by differential scanning calorimetry (DSC) and dynamic mechanical analysis (DMA). The latter allows the calculation of the molar masses M_c of the polymer chains between the network junction points. The mobility of the charge carriers in relation to the plasticizer was studied by pulsed field gradient NMR (PFG NMR). The combination of these techniques allows us to explain the ionic conductivity of these materials with dependence on the gel structure.

2. Experimental Section

2.1. Materials and Film Preparation. (EG)$_n$DME with molar masses between 134 and 2000 g/mol and $LiCF_3SO_3$ were purchased from Fluka. MAN was used after sublimation. (EG)$_4$DVE was obtained from the BASF AG.

Films of 100−300 μm thickness were prepared by in situ photopolymerization. MAN and (EG)$_4$DVE were used in the molar ratio of 2:1. The mixture of monomers, plasticizer, and salt covered by a Teflon foil was polymerized on a Teflon dish by irradiation with ultraviolet light (λ_{max} = 254 and 366 nm) at a distance of 5 cm at room temperature in an argon-filled glovebox for 15 min. No photoinitiator was necessary. To complete the conversion, all films were annealed at 80 °C overnight. The C=C double bond conversion was checked by Raman spectroscopy. No analyzable ν(C=C) modes could be detected in the gel electrolyte films. Details are given in ref 18.

2.2. DSC and DMA Measurements. For the study of the thermal properties, a differential scanning calorimeter, DSC 220 C (SEIKO Instruments Inc.) was used. The measurements were performed with samples of 5−10 mg in Al pans between −110 and +200 °C with a heating rate of 10 K/min.

Dynamic mechanical measurements were performed by a DMA 242/1/F from NETZSCH between −100 and +200 °C. Specimens with a diameter of 10 mm and a highness of 1−2 mm were prepared by UV irradiation for 2 h and annealing at 80 °C for 12 h. Generally, the compression modus was used, mainly with the following parameters: limit dynamic force 6 N, frequency 1 Hz, amplitude 60 μm, heating rate 3 K/min.

To estimate the cross-linking density of the polymer networks, the molar masses M_c of the chains between the network junction points were determined. M_c was calculated from the dynamic storage modulus E', which was measured for fully extracted and dried samples at a temperature $T = T_g + 60$ K by DMA in the compression mode. The plasticizer and the salt were extracted with THF from the gels. The following equation was used under the assumption of the nonaffine phantom model[20]

$$G = \frac{(f-2)}{f}\left(\frac{\rho RT}{M_c}\right) \tag{1}$$

with G' the shear modulus, f the functionality, and ρ the density. G' was calculated from the dynamic storage modulus E' with $G' = E'/3$.[20] A functionality f of the network junction points of $f = 3$ was assumed, referring to the high content of cross-linking monomers in the reaction mixture. M_c(calc) was calculated from the molar masses of the two monomers and their molar ratio under the assumption of the formation of an ideal network. For further details see refs 17−19.

2.3. Positron Annihilation Lifetime Spectroscopy and Spectral Analysis. In the PAL spectroscopy experiment, positron lifetime measurements were carried out using a conventional fast−fast coincidence system[3,7] with a time resolution of 260 ps (full width at half-maximum of a Gaussian resolution function) and a channel width of 50−52 ps.

The ^{22}Na positron source with an activity of 2×10^6 Bq was made by evaporating carrier-free ^{22}NaCl solution on a Kapton film of 8 μm thickness. The ^{22}Na nucleus emits a 1.28 MeV γ-ray simultaneously (within a few picoseconds) with the positron. The positron lifetime is determined from the time delay between the emission of the birth γ (1.28 MeV) and one of the 0.51 MeV annihilation quanta.[3,7] For each experiment, two identical samples (1−1.5 mm thickness) were sandwiched around the positron source. The lifetime spectra of polymers and of the reference material (pure, well annealed aluminum, τ_{Al} = 162 ps) were measured over a period of 2 h for getting the standard statistical accuracy of 2 million total count within a spectrum. Some selected samples were measured with a very high accuracy of 16 million total count. While the lifetime of an individual positron may vary between 0 and ∞, the lifetime spectrum of an ensemble of positrons annihilating from a unitary state is a single-exponential function $\exp(-t/\tau)$. τ denotes the mean lifetime of the positrons which responds inversely to the electron density at the positron site.[3,7] The lifetime spectra were analyzed using the routines LIFSPECFIT[21] and MELT.[22]

In the conventional, discrete-term routine LIFSPECFIT, the positron lifetime spectrum $s(t)$ is represented by a sum of

negative exponentials:[3,7]

$$s(t) = \Sigma \frac{I_i}{\tau_i} \exp\left(-\frac{t}{\tau_i}\right) \quad (2)$$

where τ_i is the positron lifetime in the ith state with a relative intensity I_i, $\Sigma I_i = 1$. Analysis involves least-squares fitting of eq 2, during which the number of exponential terms has to be assumed, following convolution with the experimental resolution. In addition, a commonly used correction procedure for positrons annihilating within the source and the containing materials was applied (380 ps/4%, Kapton foil and NaCl; 2500 ps/0.5%, surface effects). Three or sometimes four components are resolved in the lifetime spectra of the gel electrolyte samples. The routine MELT (Maximum Entropy for Lifetime analysis) assumes a continuous lifetime distribution.

$$s(t) = \int \frac{I(\tau)}{\tau} \exp\left(-\frac{t}{\tau}\right) d\tau \quad (3)$$

and inverts $s(t)$ into $I(\tau)$ via a quantified maximum entropy method. Unlike the discrete-term analysis it does not require any assumptions concerning the shape of $I(\tau)$ or the number of components. However, a large total count of at least 1×10^7 is typically necessary with MELT in order to obtain sufficient sensitivity to the shape of the distribution.[23,24]

2.4. PFG NMR Experiments. ^{1}H, ^{19}F, and ^{7}Li PFG NMR experiments were carried out with the home-built spectrometer FEGRIS 400 (^{1}H-resonance frequency of 400 MHz) to measure the self-diffusion coefficients D of the plasticizer and the cations and the anions in the gel.[25,26]

The self-diffusivity D was calculated from the spin echo attenuation $S_{inc}(q,t)$ of the ^{1}H, ^{19}F, and ^{7}Li nuclei with dependence on the applied field gradients. A detailed description of this method can be found in ref 27.

The NMR signal was generated by the stimulated-echo rf-pulse sequence: $\pi/2-\tau-\pi/2-t'-\pi/2-\tau-$echo, with field gradient pulses (amplitude g, duration δ) applied after the first and third rf-pulses. In each experimental run, τ was chosen to be 3 ms, t was fixed (typically 50 ms), and g was incremented. The maximum g value was 25 T m^{-1}, and the maximum δ value was 1.85 ms. The space window of PFG NMR covers a region between $1/q_{max} \approx 80$ nm and a few micrometers.

The measured spin echo attenuation A/A_0 is equivalent to the incoherent intermediate scattering function known from neutron scattering:[28]

$$\frac{A}{A_0} = S_{inc}(q,t) = \int \exp(iqz)\, P(z,t)\, dz \quad (4)$$

A and A_0 are the spin echo amplitudes with and without the applied field gradients, respectively. $P(z,t)$ is the so-called propagator,[27] i.e., the probability density for a displacement of a polymer segment over the distance z within the diffusion time. With a Gaussian propagator (free diffusion), from eq 4 we obtain

$$S_{inc}(q,t) = \exp(-q^2 D t) \quad (5)$$

where D is the self-diffusion coefficient and q is the wave vector $q = \gamma\delta g$ with the gyromagnetic ratio γ. By means of the Einstein relation

$$\langle z^2 \rangle = 2Dt \quad (6)$$

the self-diffusion coefficient may be transferred into the mean square displacement $\langle z^2 \rangle$ of the polymer segments in the z-direction during the observation or diffusion time t. Equation 5 represents the so-called narrow-pulse approximation $\pi/3 \ll t$, which is fulfilled in these experiments.

Measurements dependent on the temperature were carried out with an accuracy of 1 K. The experimental error of the self-diffusion coefficients never exceeds 10%.

2.5. Conductivity Measurement. Impedance data were obtained using a combination of a potentiostat/galvanostat (model 263 A) and a frequency response analyzer (model 1025) from EG&G. The complex impedance plots of the samples were recorded in the frequency range from 1 to 10^5 Hz.

The dependence of the ionic conductivity σ on the pressure p was measured with an home-built apparatus for high-pressure dielectric spectroscopy developed at the University of Ulm. Details are given in ref 29. The experimental data define straight lines in a plot of the logarithm of conductivity versus pressure. The slope of the line allows us to determine an activation volume V^* of the ionic conductivity using

$$V^* = -kT(\partial \ln \sigma/\partial p)_T \quad (7)$$

where T is the temperature and k is the Boltzmann constant. Strictly speaking, the activation volume depends not only on the pressure dependence of the conductivity but also on the compressibility of the material and on the pressure dependence of the charge carrier number. However, these latter parameters can be neglected.[47,50]

3. Results

3.1. Thermal and Structural Investigations by DMA and DSC. Table 1gives a summary of the molecular masses M_c between the network junction points for fully extracted samples prepared by photopolymerization of the monomers in the presence of a solution of $LiCF_3SO_3$ in $(EG)_{11}DME$ and for samples prepared by photopolymerization in bulk. Generally, a high network density was observed.

A relatively good correspondence was found for poly(MAN-*alt*-$(EG)_4$DVE) obtained by bulk polymerization between the experimentally determined M_c(exp) calculated by eq 1 and M_c(calc) calculated from the molar mass of the monomers under the assumption of the formation of an ideal network. For gel electrolyte networks, M_c(exp) determined after extraction of the plasticizer−salt solution was found to be higher than calculated.

The DSC plots of the gel electrolytes containing $(EG)_{11}DME$ indicate the glass transition and the melting of the plasticizer−salt solution at approximately −67 °C and −15 °C (onset), respectively (Figure 1a). No signals, neither the glass transition nor the melting of the plasticizer were observed in the DSC plots of gels containing $(EG)_4DME$ (not shown), although the solution of $LiCF_3SO_3$ in $(EG)_4DME$ shows a melting process at −34 °C. Hence, it can be concluded that the presence of the polymer network and the salt reduce the crystallinity of the dimethyl ether.[18,42] Completely amorphous gels were obtained with $(EG)_4DME$. The glass transition of the polymer could not be detected by DSC. This is a well-known problem of the characterization of polymer networks caused by the high network density.

However, the glass transition of the polymer was clearly detected by DMA (maximum of tan δ) (Figure 1b) as well as for samples polymerized in bulk and for the gels containing $(EG)_{11}DME$ (Figure 1b and Table 1) and $(EG)_4DME$ (Table 1), respectively. After extraction of the plasticizer−salt solution, the DMA plot shows the signal of the polymer shifted to a

TABLE 1: M_c and T_g of Poly(MAN-*alt*-(EG)$_4$DVE) Gels with 0.6 mol/kg $LiCF_3SO_3$ as well as M_c and T_g of the Copolymer Networks Determined after Extraction of (EG)$_n$DME and Salt

(EG)$_n$DME *n*	wt % plast	M_c(calc) (g/mol)	M_c(exp) (g/mol)	T_g (°C) (tan δ_{max}) of the extracted gel	T_g (°C) (tan δ_{max}) of the polymer in the gel electrolyte
		172	100	114 (0.26)[a]	
11	50	172	670	103 (0.38)	95 (0.18)
11	60	172	600	103 (0.41)	101 (0.39)
11	75	172	620	110 (0.46)	101 (0.50)
4	50	172	1420	120 (0.41)	99 (0.26)
4	65	172	1120	110 (0.48)	

[a] Bulk polymerization.

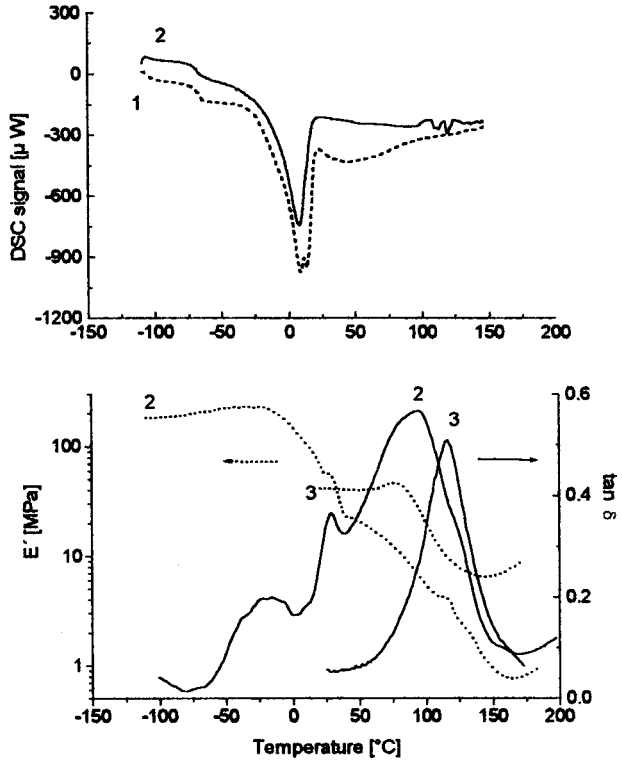

Figure 1. DSC and DMA plots of (1) 0.74 mol/kg $LiCF_3SO_3$ in (EG)$_{11}$DME, (2) poly(MAN-*alt*-(EG)$_4$DVE), 75 wt % (EG)$_{11}$DME, 0.6 mol/kg $LiCF_3SO_3$, and (3) poly(MAN-*alt*-(EG)$_4$DVE) after extraction of 75 wt % (EG)$_{11}$DME and 0.6 mol/kg $LiCF_3SO_3$.

slightly enhanced temperature. Two additional signals can be observed in the DMA plot of the gel electrolytes containing (EG)$_{11}$DME, which are related to the glass transition and the melting of the plasticizer considering the DSC results (Figure 1a,b).

3.2. PAL Spectroscopy. Two typical positron lifetime spectra are shown in Figure 2. Three components are resolved in the lifetime spectra with lifetimes of $\tau_1 = 195-205$ ps, $\tau_2 = 385-400$ ps, and $\tau_3 = 1.8-2.6$ ns related to the p-Ps self-annihilation, the annihilation of free positron (not Ps), and the o-Ps annihilation, respectively. Only the o-Ps lifetime component clearly responds to material properties and increases from $\tau_3 = 1790 \pm 20$ ps/$I_3 = 14.0 \pm 0.5\%$ in pure poly(MAN-*alt*-(EG)$_4$DVE) to $\tau_3 = 2420 \pm 20$ ps/$I_3 = 17{,}2 \pm 0.3\%$ in poly(MAN-*alt*-(EG)$_4$DVE) with 65 wt % (EG)$_{11}$DME. The variance (goodness) of the fit increases from 1.06 (ideal value 1.0 ± 0.07) in pure poly(MAN-*alt*-(EG)$_4$DVE) to 1.5, indicating that the model function does not perfectly describe the features of the experimental spectrum of the polymer containing plasticizer. A fit of these spectra with eq 2 assuming four exponential terms gives the ideal variance of fit (1.02) and two o-Ps lifetimes of approximately $\tau_{3(I)} = 1800$ ps and $\tau_{3(II)} = 2700$ ps.

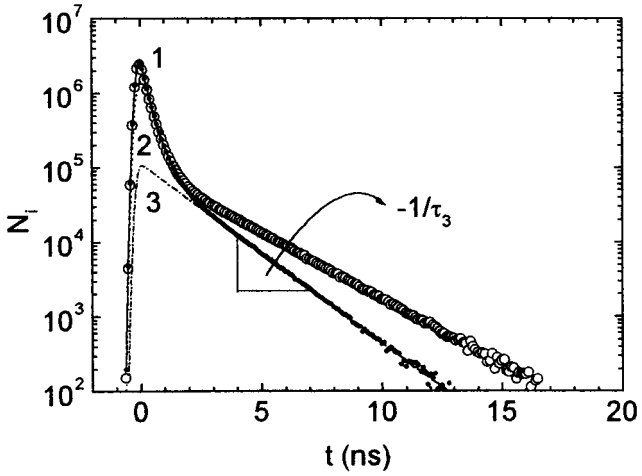

Figure 2. Positron lifetime spectra $s(t)$ of poly(MAN-*alt*-(EG)$_4$DVE) without (filled circles) and with 65 mass % (EG)$_{11}$DME (empty circles, 16 million total count). The number of annihilation events N_i in the channel i is shown as a function of the time delay t between birth and annihilation of positrons. The experimental data are displayed after subtraction of the background and source components. The spectra consist of a superposition of three exponential components (1−3) with the slopes $-1/\tau_i$. The analyzed lifetimes amount to $\tau_1 \approx 200$ ps, $\tau_2 \approx 400$ ps, and $\tau_3 = 1790$ ps (filled circles). Only the third (o-Ps) component clearly responds to material properties and increases due to plastication to $\tau_3 = 2420$ ps (open circles, see text).

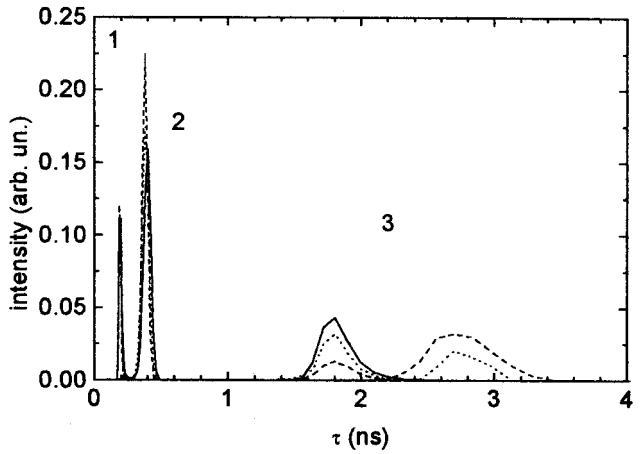

Figure 3. Positron lifetime distribution $I(\tau)$ in poly(MAN-*alt*-(EG)$_4$DVE) without (solid line) and with 35 wt % (dotted line) and 65 wt % (EG)$_{11}$DME (dashed line). The distributions where obtained from $1{,}6 \times 10^7$ count spectra using the MELT routine.

Three lifetime spectra each of them measured with a total count of 16 million were analyzed using the routine MELT (entropy weight 2×10^{-7}). As can be observed in Figure 3, three peaks appear in the positron lifetime distribution again related to the annihilation of p-Ps (1), of free positrons (2), and of o-Ps (3), respectively. Peak (3) splits into two subpeaks. The

TABLE 2: Lifetime I and Intensity τ Determined for the o-Ps Annihilation in 16 Million Count PAL Spectra of Poly(MAN-*alt*-(EG)$_4$DVE) Containing Different Amounts of (EG)$_{11}$DME

% (EG)$_{11}$DME	$\tau_{3(I)}$ (ps)	$I_{3(I)}$ (%)	$\tau_{3(II)}$ (ps)	$I_{3(I)}$ (%)
–	1830	13.7 (± 0.3)	–	–
35	1803	9.5 (± 2.0)	2760	5.7 (± 2.0)
65	1810	4.2 (± 2.0)	2740	14.5 (± 2.0)

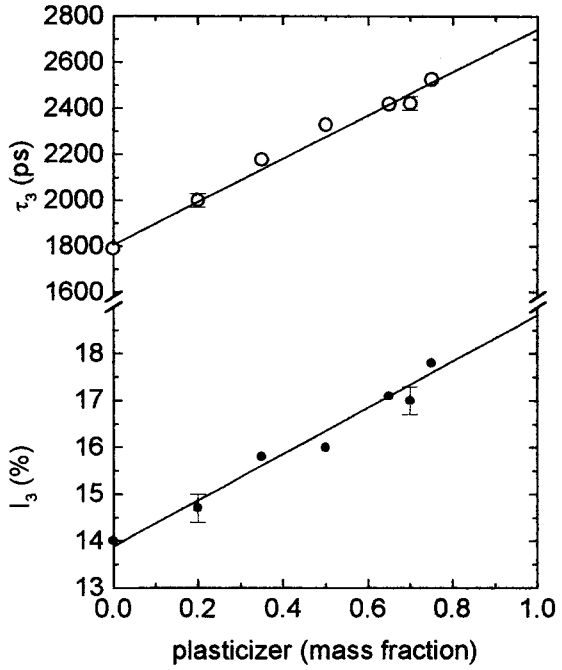

Figure 4. o-Ps lifetime τ_3 and intensity I_3 in poly(MAN-*alt*-(EG)$_4$DVE) as a function of the concentration of (EG)$_{11}$DME.

characteristic lifetime τ_i of each annihilation channel was calculated from its mass center and its weight intensity I_i from the relative area below the corresponding peak (Table 2). Within the error limits they agree with the parameters obtained from the three and four discrete term fits, respectively (for more details see refs 23 and 24). The o-Ps parameters $\tau_{3(I)}/I_{3(I)}$ and $\tau_{3(II)}/I_{3(II)}$ are rather inaccurate due to their small separation when four lifetimes were resolved in the discrete or continuous spectrum analysis. Therefore, we analyzed finally all spectra assuming three discrete lifetime components. This provided us with parameters of highest statistical accuracy. $\tau_{3(I)}/I_{3(I)}$ increases linearly with increasing content of plasticizer in the polymer (Figure 4). The parameters τ_3/I_3 are shown in Figure 5 as a function of the concentration of the conducting salt. I_3 decreases more or less pronounced, while τ_3 may slightly decrease or increase.

3.3. Self-Diffusivity and Conductivity. A typical example of an echo attenuation plot is shown in Figure 6. The curvature shows a slight deviation from a single exponentional behavior of the spin echo attenuation $S_{inc}(q,t)$. Therefore, it was fitted with a stretching exponential function, a Kohlrausch−Williams−Watt equation:

$$S_{inc}(q,t) = \exp(-(q^2tD)^{\beta}) \qquad (8)$$

β characterizes the width of the distribution. It varied between 0.8 and 1. $\beta = 1$ means exponential behavior.

The dependence of the diffusion of the charge carriers on the diffusivities of (EG)$_n$DME and its molar mass in poly(MAN-*alt*-(EG)$_4$DVE) networks was studied. Charge carrier and plasticizer diffusion are related (Figures 7 and 8), as can be

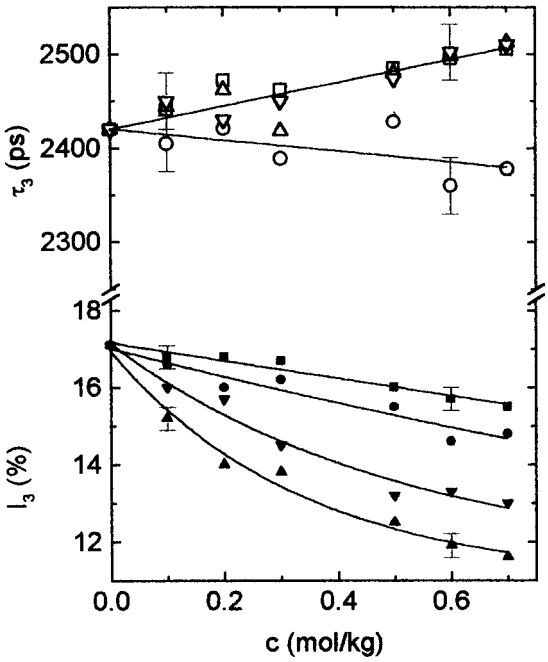

Figure 5. o-Ps lifetime τ_3 and intensity I_3 in poly(MAN-*alt*-(EG)$_4$DVE) with 65 wt % (EG)$_{11}$DME as a function of the concentration of the conducting salt: $LiCF_3SO_3$ (squares); $LiClO_4$ (circles); $LiPF_6$ (down triangles); $LiN(CF_3SO_2)_2$ (up triangles).

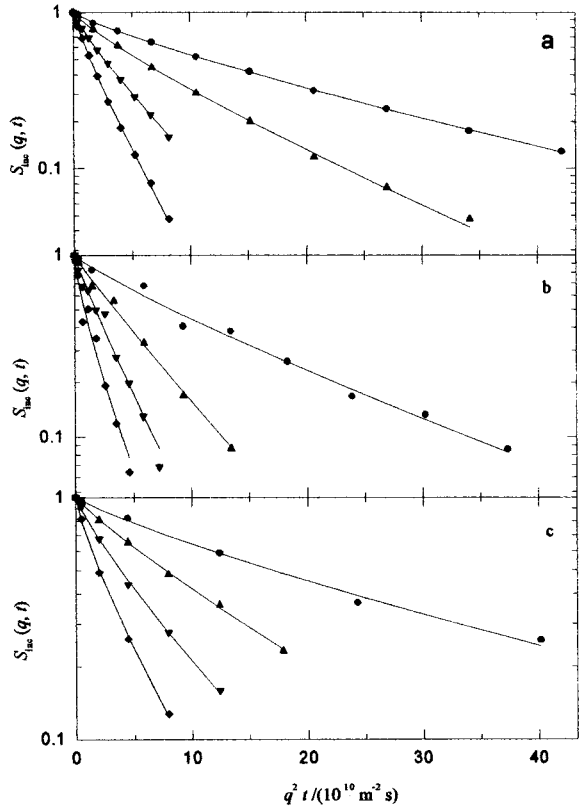

Figure 6. Echo attenuation plot for (a) ^{1}H, (b) ^{19}F, and (c) ^{7}Li NMR of a gel electrolyte on the basis of poly(MAN-*alt*-(EG)$_4$DVE) containing 75 wt % (EG)$_{11}$DME and 0.6 mol/kg $LiCF_3SO_3$, at (●) 20, (▲) 40, (▼) 60, and (◆) 80 °C.

expected from the literature.[38−40,42] In correspondence with the literature[38−40,42] the following sequence was commonly found $D_{exp}(H) > D_{exp}(F) > D_{exp}(Li)$. The measured self-diffusivities $D_{exp}(Li)$, $D_{exp}(F)$, and $D_{exp}(H)$ are averaged values. The nuclei studied by PFG NMR are part of different ionic species due to

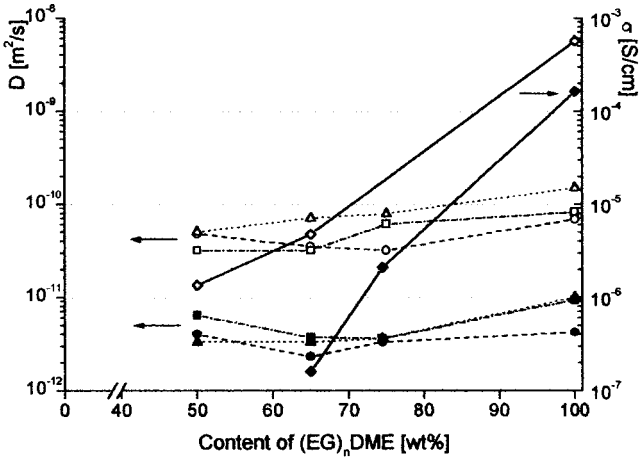

Figure 7. Ionic conductivity and D_{exp}(H) (triangles), D_{exp}(F) (squares), and D_{exp}(Li) (circles) as a function of the $(EG)_n$DME content ($n = 4$, open symbols, and 11, filled symbols) in the gel electrolytes on the basis of poly(MAN-*alt*-$(EG)_4$DVE), $c_{LiCF3SO3} = 0.6$ mol/kg, 20 °C

ionic association and interaction of the charge carriers with the plasticizer and the polymer. Despite this, a single self-diffusion coefficient is observed because of a fast exchange between the different ionic states, faster than the time scale of the diffusion measurements.[38−40,42]

In Figure 8 the exponent α for the relationship $D \sim M^{-\alpha}$ is indicated. Surprisingly, α was found to be generally larger than 2 for all measured D in the temperature range between 20 and 80 °C. Only for $T = 80$ °C does α become smaller than 2 in the case of the charge carrier diffusion. The activation energy E_A of the self-diffusivity of charge carriers and plasticizer increases with rising n of the $(EG)_n$DME and reaches a plateau for $n > 11$ (Figure 9).

The ionic conductivity decreases dramatically with decreasing content of $(EG)_{11}$DME in the poly(MAN-*alt*-$(EG)_4$DVE)-based gel electrolytes, whereas D_{exp}(Li), D_{exp}(F), and D_{exp}(H) remain relatively unchanged (Figure 7).

According to eq 7, an activation volume $V^* = 22.7$ cm^3/mol was calculated from the pressure dependence of the ionic conductivity of poly(MAN-*alt*-$(EG)_4$DVE) containing 65 wt % $(EG)_{11}$DME (Figure 10).

4. Discussion

4.1. Structure of the Polymer Gel Electrolytes. The structure of the poly(MAN-*alt*-$(EG)_4$DVE) networks exhibits typical differences caused by the different polymerization conditions (Table 1). The molar masses M_c(exp) of the network chains between the junction points determined for the copolymer obtained by polymerization in bulk agrees approximately with M_c(calc). The copolymerization in the presence of the plasticizer results in networks with distinctly higher M_c(exp). This can be explained by intramolecular reactions of pendant C═C double bonds with free-radical chain ends at the same macromolecule leading to the formation of cycles. The propability of these reactions rises with decreasing monomer concentration. This effect was found to be more pronounced if the lower viscous $(EG)_4$DME was used as a plasticizer. A similar behavior was also observed for gel electrolytes obtained by polymerization of $(EG)_n$DMA in the presence of $(EG)_{11}$DME or other plasticizers.[19]

From the thermal analysis (Figure 1a,b) it follows that gel electrolytes on the basis of poly(MAN-*alt*-$(EG)_4$DVE) are heterogeneous materials composed of a polymer network and of a liquid phase.

T_g of the cross-linked copolymers (Table 1) is obviously rather independent of the network density; i.e., it depends on the chemical composition of the copolymers, which is in all cases the same.

4.2. Local Free Volume of the Polymer Gel Electrolytes. *4.2.1. Cross-Linked Polymer with and without Plasticizer.* As can be observed in Figure 4, τ_3/I_3 increases from 1790 ps/14.0% in pure poly(MAN-*alt*-$(EG)_4$DVE) to 2730 ps/18.9% (extrapolated) in the pure $(EG)_{11}$DME. These boundary parameters agree within the error limits with o-Ps lifetime parameters $\tau_{3(I)}/I_{3(I)}$ and $\tau_{3(II)}/I_{3(II)}$ estimated via the MELT routine from the 1.6×10^7 count spectra. The appearance of the two subpeaks $\tau_{3(I)}$ and $\tau_{3(II)}$ in the lifetime distribution analyzed via MELT (Figure 3) and the linear behavior of o-Ps lifetime parameters τ_3 and I_3 confirm a two-phase model of o-Ps annihilation in the polymer gel: $\tau_{3(I)}/I_{3(I)}$ may be attributed to the solid polymer network and $\tau_{3(II)}/I_{3(II)}$ to the plasticizer liquid confined in the cross-linked polymer corresponding to the results of DMA measurements.

The following relations between three- and four-component lifetime parameters are valid if it is assumed that the o-Ps lifetime parameters of the polymer and the plasticizer do not change with the concentration of plasticizer in the polymer:

$$I_3 = (1 - w)I_{3(I)} + wI_{3(II)} \tag{9}$$

$$\tau_3 = [(1 - w)I_{3(I)}\tau_{3(I)} + wI_{3(II)}\tau_{3(II)}]/[(1 - w)I_{3(I)} + wI_{3(II)}] \tag{10}$$

If there is no net flow of Ps between the two phases, the polymer framework, and the plasticizer, the factor w is the volume fraction of the plasticizer, which corresponds approximately to the mass fraction. The lifetime τ_3 is the weighted average of the o-Ps lifetimes $\tau_{3(I)}$ and $\tau_{3(II)}$, with the weight factors $(1 - w)$ and w of the o-Ps formation probabilities in the constituent systems of the gel, $I_{3(I)}$ and $I_{3(II)}$.

In the following section we discuss in more detail the o-Ps annihilation mechanism that affects the values of τ_3 and I_3. Besides the pick-off annihilation, other quenching processes may occur such as ortho−para spin conversion due to internal or external magnetic fields or chemical quenching. Furthermore, o-Ps formed may decay via self-annihilation.[7] The reduction of the o-Ps lifetime τ_{o-Ps} due to the various quenching processes may be described by[9]

$$\tau_{o-Ps} = 1/(\eta\lambda_{o-Ps}{}^{o} + \lambda_{po} + \lambda_{qu}) \tag{11}$$

where $\lambda_{o-Ps}{}^{o} = (\tau_{o-Ps}{}^{o})^{-1}$ is the o-Ps self-annihilation rate ($\tau_{o-Ps}{}^{o} = 142$ ns), $\lambda_{po} = (\tau_{po})^{-1}$ is the pick-off annihilation rate, and λ_{qu} denotes the rates of all other possible quenching mechanisms. η is the so-called contact density or relaxation parameter, which describes the relaxation of Ps in matter compared with the state in a vacuum. For hydrocarbons $\eta \approx 0.8$ can be assumed.[9] The diameter of the Ps probe behaves as $0.106\ \eta^{-1/3}$ nm and the p-Ps and o-Ps lifetimes due to self-annihilation relate to η as 125 ps/η and 142 ns/η, respectively. The poly(MAN-*alt*-$(EG)_4$DVE) polymer and also the $(EG)_{11}$DME plasticizer contain only oxygen besides carbon and hydrogen. These elements do not form known Ps quenching centers. Therefore, we may assume that the pick-off annihilation of o-Ps from inside the holes in the amorphous phase is the only or dominating o-Ps quenching process.

In solids and liquids Ps is repelled by most of the molecules due to the Coulomb force and the exchange effect. The latter is a consequence of the Pauli principle. From eq 11 it follows that the observed lifetime of o-Ps confined in a hole may be

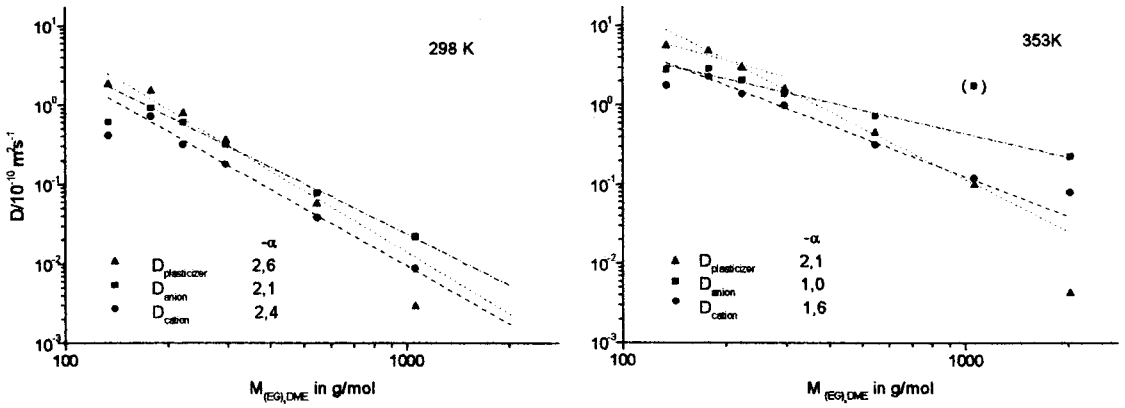

Figure 8. log−log plot of D vs M for the diffusion of charge carriers and various $(EG)_nDME$ (75 wt %) in poly(MAN-*alt*-$(EG)_4DVE$) at 298 and 353 K, respectively, $c_{LiCF3SO3} = 0.6$ mol/kg. The value of the exponent α of $M^{-\alpha}$ is indicated in the figure.

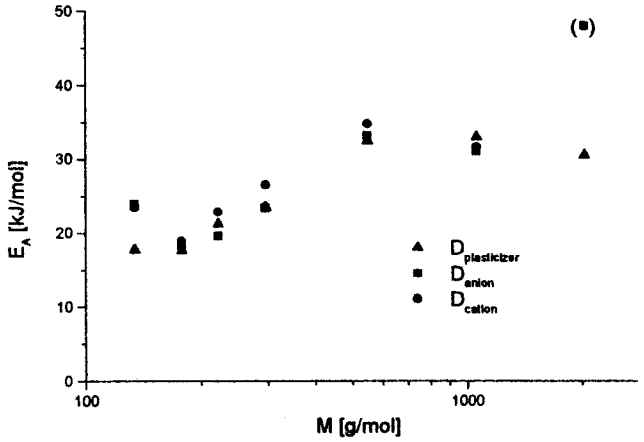

Figure 9. Activation energy E_A determined for $D_{exp}(H)$, $D_{exp}(F)$, and $D_{exp}(Li)$ for gel electrolytes on the basis of poly(MAN-*alt*-$(EG)_4DVE$) containing 75 wt % $(EG)_nDME$ and 0.6 mol/kg $LiCF_3SO_3$.

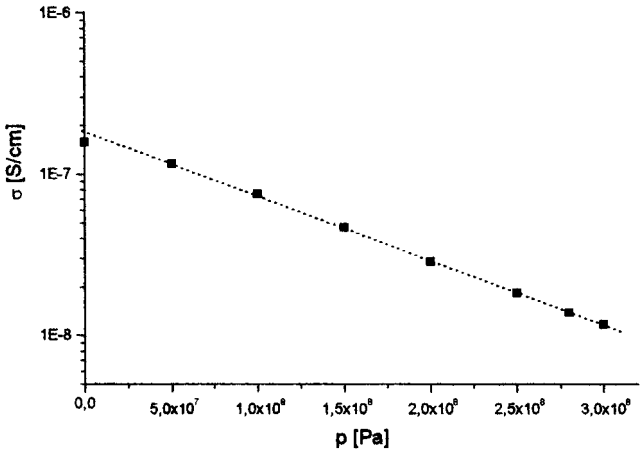

Figure 10. Ionic conductivity as a function of pressure for a gel electrolyte of poly(MAN-*alt*-$(EG)_4DVE$) containing 65 wt % $(EG)_{11}DME$ and 0.6 mol/kg $LiCF_3SO_3$.

expressed by $\tau_{o-Ps} = 1/[(1 - W)\eta\lambda_{o-Ps}{}^{o} + W\lambda_m] \approx W^{-1}\tau_m$ ($\lambda_m \gg \eta\lambda_{o-Ps}{}^{o}$). W is the fraction (weight) of Ps density that overlaps with the electron layer at the inner surface of the hole, and τ_m (λ_m) is the o-Ps lifetime (annihilation rate) inside the layer. τ_m is well approximated by the spin-averaged Ps lifetime of 0.5 ns, which is also observed in densely packed molecular crystals. For calculating the value of W, a simple quantum mechanical model is used, which assumes that the Ps is confined in a spherical potential wall of radius r and infinite depth and that the Ps has a spatial overlap with molecules within a layer dr of the potential wall. This provides a well-accepted relationship between the o-Ps pick-off lifetime, $\tau_{o-Ps} \approx \tau_{po} = \tau_m W^{-1}$, and the radius of the hole:[5,8,10]

$$\tau_{po} = 0.5ns\left[1 - \frac{r}{r+\delta r} + \frac{1}{2\pi}\sin\left(\frac{2\pi r}{r+\delta r}\right)\right]^{-1} \qquad (12)$$

By fitting eq 12 to the observed o-Ps lifetime of known mean hole radii in porous materials, $\delta r = 0.166$ nm was obtained. Thus, eq 12 represents a calibration curve for the dependence of the o-Ps lifetime on the hole radius r, which is widely used to estimate the mean size of free-volume holes in amorphous polymers.[4−10,31]

Because of the repulsion of Ps by molecules, it is generally assumed that in amorphous polymers all Ps atoms annihilate from inside a local free volume (a "hole"), e.g., cavities or holes of atomic or molecular dimensions that are due to irregular molecular packing in the amorphous phase (static and preexisting holes) and due to molecular relaxation among the molecular chains and terminal ends (dynamic and transient holes). With the assumption that o-Ps annihilation is the dominating quenching process occurring in the gel electrolytes studied, we can now estimate from the o-Ps lifetime $\tau_3 = \tau_{3(I)} = 1790 \pm 20$ ps observed for pure poly(MAN-*alt*-$(EG)_4DVE$) a hole radius of $r = 0.265 \pm 0.003$ nm using eq 9, and via $v = 4\pi r^3/3$, a hole volume of $v = 0.088 \pm 0.003$ nm^3. In view of the structure of the material, the estimated hole size is in a plausible range. The separation of neighboring carbon atoms in hydrocarbons is 0.15 nm; the bivalent CH_2 group occupies a van der Waals volume of 0.017 nm^3.[23,24] A radius of 0.2−0.25 nm has to be assumed for the maleic anhydride group.[30] Typical o-Ps lifetimes (hole radii) in glassy polymers have values of ∼1500 ps (0.23 nm, epoxy resins[32]) to ∼2000 ps (0.28 nm polycarbonate[23]) while in rubbery polymers lifetimes of 2500 ps (0.32 nm, polybutadiene[33]) and larger values may be observed.

Ps is also confined in "holes" in liquids. These holes are created by the Ps probe itself because of the high mobility of the molecules and are called Ps bubbles. Their size can be also estimated from the o-Ps lifetime via eq 12. From the o-Ps lifetime $\tau_3 = \tau_{3(II)} = 2730 \pm 30$ ps (Figure 3) obtained for the gel containing $(EG)_{11}DME$, a Ps bubble radius of $r = 0.345 \pm 0.01$ nm and a Ps bubble volume of $v = 0.172 \pm 0.01$ nm^3 were estimated. The large Ps bubble size in the plasticizer liquid, if compared with the hole size in the amorphous polymer network, can be attributed to the repulsion of the mobile molecules of the liquid by Ps atoms. In the literature, o-Ps lifetimes of Ps bubbles in liquids have been observed ranging from 1500 to 5000 ps.[7,35]

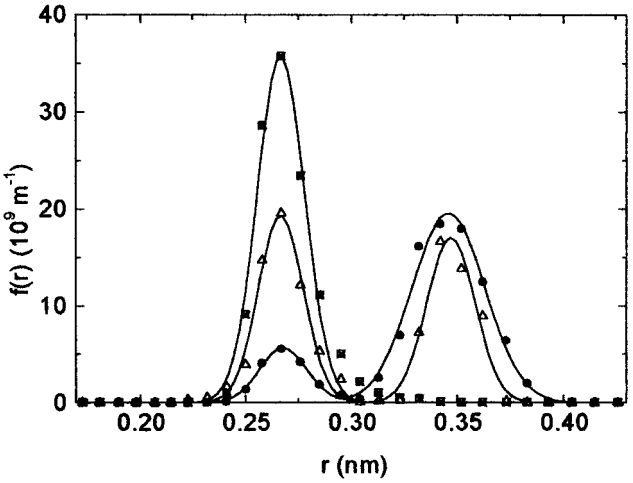

Figure 11. Hole radius distribution $f(r)$ estimated from the positron lifetime distributions shown in Figure 3.

In a bubble state the inward pressure due to the surface tension is counterbalanced by the outward pressure due to the Ps−molecule repulsion and the zero point energy of the Ps (Heisenberg uncertainty principle). Assuming that the Ps is situated in a square well potential of depth U and radius r in the liquid, the total energy in the bubble state is (see, for example, refs 7, 9, and 35)

$$E = E_0(U,r) + 4\pi r^2\gamma + {}^4/_3\pi p r^3 \quad (13)$$

$E_0(U,r)$ is the Ps zero point energy in the potential, the second and third terms are the surface (γ, surface tension) and pressure−time−volume energies, respectively. Assuming that the square well has infinitely high potential walls and that the pr^3 term is insignificant as it is normally found, we get from the equilibrium condition $dE/dr = 0$ the relation

$$r\,(\mathrm{nm}) = (\pi^2\hbar/16m_e)^{1/4}\gamma^{-1/4} = 1.241\gamma\,(\mathrm{dyn/cm})^{-1/4} \quad (14)$$

for the equilibrium radius of the bubble.[24] Here $\hbar$ is Planck's constant and m_e is the mass of an electron (positron). An empirical relation (15) between the macroscopic surface tension γ and the o-Ps pick-off lifetime τ_{o-Ps} has been found by Tao:[34]

$$\tau_{o-Ps}\,(\mathrm{ns}) = (k\gamma^n)^{-1} \quad (15)$$

where for n-alkanes values of $k = 0.061$ and $n = 0.50$ and for oxygenated short-chain hydrocarbons $k = 0.046$ and $n = 0.55$ have been determined (γ is given in dyn/cm).

From the Ps bubble radius of $r = 0.345$ nm a surface tension of $\gamma = 166$ dyn/cm may be estimated using eq 14, which is much higher than the macroscopic surface tension of "free" $(EG)_n$DME of usually 28−44 dyn/cm[36] with dependence on the molar mass. This corresponds to a Ps bubble radius between 0.48 and 0.59 nm.

The unexpected low Ps bubble radius is probably the consequence of the "confinement" of $(EG)_{11}$DME in the highly cross-linked polymer network, which may lead to a lower mobility of liquid molecules and to an increase in the internal pressure of the liquid compared to that of the "free liquid". An increase in the $p\upsilon = {}^4/_3\pi r^3 p$ term in eq 13 would lead to a lower Ps bubble radius r.

If the unique correspondence of the o-Ps lifetime and the free-volume hole radius given by eq 12 is assumed to be valid, the lifetime distribution estimated via the MELT routine (Figure 3) may be transformed into a hole radii distribution (Figure 11). An expression for the probability density function of the hole radii $f(r)$ is derived as

$$f(r) = -3.32\{\cos[2\pi r/(r+\delta r)] - 1\}I(\tau)\tau^2/(r+\delta r)^2 \quad (16)$$

where r is the radius of an individual local hole of the free volume and $\delta r = 0.166$ nm.[8,9] The fraction of o-Ps annihilation in the holes with radii between r and $r + dr$ is $f(r)\,dr$. $f(r)$ has been normalized so that $\int f(r)\,dr = 1$ (integration from 0 to ∞). Analogous to the o-Ps lifetimes, the hole sizes show a bimodal distribution (Figure 11). As already discussed, the smaller holes are local free volumes in the amorphous polymer network, while the large holes are Ps bubbles formed in the plasticizer liquid. The mass centers of the distributions agree with the mean hole radii of $r = 0.265$ and 0.345 nm estimated previously from the discrete (mean) values of the o-Ps lifetime τ_3.

4.2.2. Polymer Electrolytes. Poly(MAN-*alt*-$(EG)_4$DVE) containing 65 wt % of $(EG)_{11}$DME was selected to study the effect of various salts ($LiCF_3SO_3$, $LiClO_4$, $LiPF_6$, and $LiN(CF_3SO_2)_2$) on the o-Ps lifetime τ_3 and its intensity I_3 in polymer gels. The estimated τ_3 may be considered as an average of the o-Ps lifetime in the polymer network and in the liquid plasticizer containing the solvated salt.

τ_3 of the polymer gel containing $LiClO_4$ decreases slightly with the increase in the salt content (Figure 5). For all other gel electrolytes under investigation τ_3 exhibits a linear increase from 2420 ps (no salt) to 2510 ps (0.7 mol/kg salt). This behavior is contrary to that found by Wang et al.[12] and Furtado et al.[51] Both described a clear decrease of τ_3 with increasing concentration of $LiClO_4$ in poly(ether urethanes). However, these systems were conventional solid electrolytes. The observed increase in τ_3 with increasing salt concentration for the gel electrolytes studied in this work may be attributed to a decreased pick-off annihilation rate of o-Ps caused by an increase of the Ps bubble size, which is explicable with a decrease of the microscopic surface tension of the liquid in the gel (eq 12 and 14). Since only $LiClO_4$ leads to a very weak decrease in τ_3, quenching effects such as chemical quenching or spin conversion seem to play no role in these gel electrolytes.

However, changes in the o-Ps lifetime should not result in changes of the intensities of the lifetime components I_3, as observed (Figure 5), if further quenching processes besides pick-off annihilation can be ruled out.

Besides quenching, inhibition processes can influence the o-Ps intensity.[7] When a fast positron penetrates a polymer it loses energy by ionization and excitation of molecules. The thermalized positron may react with a free electron to form Ps, $e^+ + e^- \rightarrow$ Ps in the last part of the ionization path (spur model[7]). This process competes with the recombination of ionized molecules with free electrons, $M^+ + e^- \rightarrow M$, and with trapping of free electrons and/or positrons by scavengers. Possible processes in the gel electrolytes studied may be the formation of complexes $e^+ + X^- \rightarrow [e^+, X^-]$ where X^- denotes the anion of a conducting salt and the recombination reaction $e^- + Li^+ \rightarrow$ Li, which is rather improbable for alkali-metal cations. Any change in the intensity of these processes may lead to a decrease (inhibition) or increase (anti-inhibition) of the Ps formation probability P. The intensities of the o-Ps component I_3 decrease or increase like the Ps yield P, $I_3 = {}^3/_4P$, but the lifetime τ_3 will not change.

The behavior of I_3 at different salt concentrations c may be phenomenologically fitted with a decreasing exponential function, $I_3(c) = I_3(0) + \Delta I_3[\exp(-c/c_s) - 1]$, where c_s is the decay constant and $\Delta I_3 = I_3(0) - I_3(\infty)$, or with the inhibition relation $I_3(c) = I_3(0) + \Delta I_3[(1+\kappa)^{-1} - 1]$ (see Mogensen,[7] eq 7.33),

with the inhibition rate κ assumed to be proportional to the concentration of the salt, $\kappa = kc$, and the rate constant k.

Differences in the behavior of I_3 for different salt−plasticizer solutions could be caused by different values of the o-Ps intensity I_3 for high salt concentrations, and the inhibition rate constant κ. Assuming that the inhibition is due to positron capture by anions only, κ is related to the capture rate. It is a function of both the type of anions and solution. Information for our system seems to be not available in the literature. Wang et al.[12] and Forsyth et al.[14] have also observed a decrease of I_3 with increasing $LiClO_4$ salt concentration in poly(ether urethane) and attributed this to a decreasing number of free volume sites. Recently, it was shown that the o-Ps intensity is not directly related to the number density of free volume or Ps bubbles.[52]

4.3. Self-Diffusivity of Ions and Plasticizer and Ionic Conductivity of the Gel Electrolytes. In correspondence with the results of the thermal analysis and PAL spectroscopy the slight deviation from the single exponential behavior of the spin echo attenuation for the electrolyte gels (Figure 6) is explicable with the heterogeneity of the material. In this case, the diffusion coefficients D should show a dependence on the time. A slight time dependence of all three measured self-diffusion coefficients (D_{exp}(Li), D_{exp}(F), and D_{exp}(H)) was indeed found for heterogeneous gel electrolytes on the basis of terpolymers from MAN and $(EG)_4$DVE with ethoxy tri(ethylene glycol) methacrylate.[37]

The conductivity of the studied gel electrolytes increases by orders of magnitude (Figure 7) with increasing content of $(EG)_n$DME, $n = 4$ and 11. However, the self-diffusion coefficients of charge carriers and plasticizer were found to be not significantly influenced by the amount of the plasticizer. The difference in the dependence of the ionic conductivity and the charge carrier self-diffusivity on the content of $(EG)_{11}$DME indicates that the Nernst−Einstein equation does not hold for the gel electrolytes studied. This behavior was previously discussed in ref 17 and explained by the heterogeneity of the electrolyte system. Whereas the conductivity is a macroscopic quantity, PFG NMR used to study the self-diffusivity has a length scale between 100 nm and a few micrometers only and records obviously pores occupied by the liquid phase of these heterogeneous gel electrolyte systems.[17] A location of the charge carriers mainly in the liquid phase is indicated by Raman spectroscopic investigations. In gel electrolytes based on poly(MAN-*alt*-$(EG)_4$DVE) containing $(EG)_{11}$DME, a high content of symmetrical LiO complexes was observed, which can only be formed by interactions between plasticizer and cations.[17]

Furthermore, it may be supposed that the gel structure formed does not provide sufficient contact of the liquid domains in the studied electrolytes, causing the disproportionately low conductivity compared with the self-diffusivity of the charge carriers. This was also indicated by the temperature dependence of the ionic conductivity.[17] The Arrhenius plots showed a nonlinear behavior with a jump at temperatures between 35 and 50 °C in the case of the studied gel electrolytes, which was explained by a successive softening of the polymer chains of the network (T_g ca. 100 °C) providing a homogenization of the material.[17] This behavior dissappeared when terpolymers of MAN and $(EG)_4$DVE with ethoxy tri(ethylene glycol) methacrylate[38] with a much lower polymer density were used as a matrix for gel electrolytes.[17]

An improvement of the charge carrier transport was expected from the use of $(EG)_4$DME as a liquid component, considering its lower viscosity and the lower network density observed for poly(MAN-*alt*-$(EG)_4$DVE) polymerized in this plasticizer (Table 1). Self-diffusivity and ionic conductivity are increased compared with gels containing $(EG)_{11}$DME. However, charge carrier diffusivity and ionic conductivity are again not related according to the Nernst−Einstein equation (Figure 7).

It was expected that D is proportional to M^{-1} of the $(EG)_n$DME corresponding to a Rouse behavior of unentangled chains, as discussed for the diffusion of charge carriers in polyether-based polymer electrolytes[41] and for the diffusion of PEO[43] in the studied range of molar mass.

However, a much higher exponent $\alpha > 2$ (Figure 8) was found for the dependence of the studied self-diffusivities on the molar mass of the plasticizer at room temperature. A relationship $D \sim M^{-2}$ is given for the diffusion of polymer chains in a polymer network.[44] Hence, the high value of the exponent α in $D \sim M^{-\alpha}$ has to be interpreted as a restriction of the charge carrier and plasticizer transport by the polymer network. This is in correspondence with the unexpected low Ps bubble size in the liquid phase of the electrolytes estimated from the lifetime $\tau_{3(II)}$ of the second component of the o-Ps annihilation, indicating a confinement of $(EG)_n$DME in the polymer network, as discussed above.

The question is, to what extent can the dependence of the self-diffusivity on the molar mass of the plasticizer be influenced by salt−plasticizer or salt−polymer interactions. It should be mentioned that IR spectra indicate salt−polymer interactions by a slight shift of the ν(C═O) band of the MAN units at 1841 cm^{-1} ("in phase") and of the combined mode δ ring $+\delta$(C−H) at 1860 cm^{-1} of 6 and 4 cm^{-1}, respectively, to higher wavenumbers if the salt concentration increases. Furthermore, an increase in the content of free anions was observed for decreasing plasticizer concentration.[17,18]

The decrease of the exponent α at 80 °C (Figure 8) is explicable by the homogenization of the sample with increasing temperature due to the softening of the polymer network (T_g = 100 °C), as discussed in connection with the shape of the Arrhenius plots of the ionic conductivity.[17]

For gel electrolytes with $(EG)_n$DME with a molar mass greater than 1000 g/mol (Figure 8) but also for the gels with a very low $(EG)_{11}$DME content (Figure 7) a faster charge carrier diffusion than plasticizer diffusion was observed, which is quite unusual compared with the literature.[38−40,42] Changes in the self-diffusivity of charge carriers and plasticizer for gels containing $(EG)_n$DME with higher molar mass are also indicated by the trend of the activation energy E_A of the self-diffusivity (Figure 9). However, this behavior is quite plausible considering that, with increasing chain length of $(EG)_n$DME, the mobility of the plasticizer molecules coordinated with cations should be dramatically reduced compared to the mobility of ionic associates, especially if one or more cations coordinate more than one plasticizer molecule. As indicated in Figure 8, anions should show the highest self-diffusion coefficient due to the low interactions with polymer and plasticizer. Cations should show an intermediate diffusivity between D_{exp}(F) and D_{exp}(H) due to the contribution of the cations in ionic associates to D_{exp}(Li).

An unusual behavior of the self-diffusivity of charge carriers and plasticizer and its activation energy E_A is also observed for gel electrolytes containing $(EG)_2$DME as a plasticizer (Figures 8 and 9). D_{exp}(Li) and D_{exp}(F) are distinctly reduced, and its E_A is increased compared with the other gel electrolytes. This can be explained with the disproportionately high degree of ionic association in solutions of $LiCF_3SO_3$ in $(EG)_2$DME. Contrary to the case with $(EG)_{11}$DME solutions, higher ionic aggregates were detected in addition to ion pairs.[45] The charge carriers are not sufficiently separated despite the formation of symmetrical LiO_6 complexes by coordination of one Li cation with two

molecules of $(EG)_2DME$, as indicated by a high intensity of the symmetrical LiO_6 breathing mode in the Raman spectra.[45] Possibly, the lower screening ability of $(EG)_2DME$ provides an enhancement of interactions of the charge carriers with the polymer, which is indicated for gels containing $(EG)_{11}DME$,[18] as mentioned above.

An activation volume of 22.7 cm^3/mol was determined from the pressure dependence of the ionic conductivity (Figure 10). Fontanella and Wintersgill found activation volumina between 30 and 40 cm^3/mol[47] for polymer electrolytes on the basis of high molecular mass PEO below the melting point. However, Duclot et al.[50] recently reported an activation volume of ca. 22 cm^3/mol (25 °C) for the Li^+ ion conductivity of solid state single ion conductors on the basis of fully amorphous cross-linked polyether networks, which should not be distinctly changed in the presence of anions, because anions have a smaller solvation shell than cations, as observed for solutions of $LiCF_3SO_3$ in $(EG)_{11}DME$.[46] Distinctly lower values (11−17 cm^3/mol) were calculated for gel electrolytes on the basis of PAN or PVDF with PC or DMC.[48,49] Therefore, the activation volume determined for the gel electrolyte on the basis of poly(MAN-*alt*-$(EG)_4$DVE) (Figure 10) has to be considered as an indication of charge carrier transport mainly occurring via the liquid phase of the gel.

The activation volume of 22.7 cm^3/mol corresponds to a hole radius of 0.21 nm, which is smaller than the hole radius of the polymer of 0.265 nm determined by PAL spectroscopy. For comparison, solvated Li cations in solutions of $LiCF_3SO_3$ in $(EG)_n$DME with $n = 4$ and 11 have Stokes' radii of 0.63 and 0.69 nm, respectively ($[EG]/[LiCF_3SO_3] = 25$).[38,46] This likewise suggests that the charge carrier transport in heterogeneous electrolytes of poly(MAN-*alt*-$(EG)_4$DVE) occurs via the liquid phase of the gels.

5. Conclusions

The polymer and gel structure of gel electrolytes of poly(MAN-*alt*-$(EG)_4$DVE) containing $(EG)_n$DME and $LiCF_3SO_3$ were studied.

These gel electrolytes are heterogeneous materials composed of a highly cross-linked polymer network and a liquid phase, the plasticizer−salt solution. The glass transition of the polymer and the liquid are separately detectable. In accordance with this, two values were determined for the size of the local free volume (mean hole radius r) for salt-free gels by PAL spectroscopy: one with $r \approx 0.26$ nm related to the polymer and a greater one with $r \approx 0.34$ nm related to the liquid phase.

We assume that the charge carrier transport occurs via the liquid phase of the electrolytes, as concluded from the low influence of the polymer network on the plasticizer diffusion and the low activation volume determined by pressure dependent conductivity measurements. However, the absence of a relation between conductivity and self-diffusivity according to the Nernst−Einstein equation, the unexpected low Ps bubble size in the liquid phase as determined by PAL spectroscopy, and the observed dependence of the self-diffusion coefficients of charge carriers and plasticizer on the molar mass of the latter indicate that the polymer structure of poly(MAN-*alt*-$(EG)_4$DVE) is too dense to provide an optimal distribution and mobility of the liquid phase. Hence, the ionic conductivities are rather low.

The presence of a salt in the studied gel electrolytes leads to a slight decrease of the microscopic surface tension of the liquid, indicated by a small increase in the o-Ps lifetime τ_3. The variation of its intensity I_3 with the concentration of the salt is caused by inhibition processes depending on the type of the salt.

Acknowledgment. We thank the Bundesministerium für Bildung und Forschung of the German Government and the BASF-AG as well as the Deutsche Forschungsgemeinschaft (SFB 294) for financial support. Moreover, we acknowledge generous financial support from the EPSRC, U.K. G.D. wishes to thank the University of Bristol for the appointment as a Benjamin Maker visiting professor.

References and Notes

(1) Doolittle, A. K. *J. Appl. Phys.* **1951**, *21*, 1471.
(2) Cohen, M. H.; Turnbull, D. *J. Chem. Phys.* **1959**, *31*, 1164.
(3) Dupasquier, A., Mills, A. T. Jr., Eds. Positron Spectroscopy of Solids. *Proceedings of the International School "Enrico Fermi"*, July 1993, Varenna, Italy; IOS Press: Amsterdam, 1995.
(4) Schrader, D. M., Jean, Y. C., Eds. Positron and Positronium Chemistry. *Studies in Physical and Theoretical Chemistry*; Elsevier Science Publishers: Amsterdam, 1988; p 57.
(5) Nakanishi, H. S.; Wang, J.; Jean, Y. C. In *Positron Annihilation Studies of Fluids*; Sharma, S. C., Ed.; World Scientific Publishing Co.: Singapore, 1988; p 292.
(6) Jean, Y. C., Eldrup, M. D., Schrader, M., West, R. N., Eds. *Positron Annihilation, Proceedings of the 11th International Conference*, ICPA11, 1997, Kansas City, MO; *Mater. Sci. Forum* **1998**, *255−257*.
(7) Mogensen, O. E. *Positron Annihilation in Chemistry*; Springer-Verlag: Berlin, Heidelberg, 1995.
(8) Jean, Y. C. *Microchem. J.* **1990**, *42*, 72. And In *Positron Annihilation, Proceedings of the 10th International Conference*; He, Y.-J., Cao, B.-S., Jean, Y. C., Eds.; *Mater. Sci. Forum, Trans Technol. Publ.* **1995**, *175−178*, 59.
(9) Gregory, R. B. *J. Appl. Phys.* **1991**, *70*, 4665. Gregory, R. B.; Chai, K. J. In *Positron Annihilation, Proceedings of the 9th International Conference*; Kajcsos, Z., Szeles, C., Eds.; *Mater. Sci. Forum* **1992**, *105−110* 1575.
(10) Eldrup, M.; Lightbody, D.; Sherwood, J. N. *Chem. Phys.* **1981**, *63*, 51.
(11) Wang, S. J.; Wang, B.; Li, S. Q.; Peng, Z. L. *J, Radioanal. Nucl. Chem.* **1996**, *211*, 127.
(12) Wang, S. J.; Wang, B.; Li, S. Q.; Peng, Z. L.; Dai, Y. Q.; He, Q. C.; Zhang, S. P. *Mater. Sci. Forum* **1997**, *255−257*, 46.
(13) Hill, A. J.; MacFarlane, D. R.; Li, J.; Jones, P. L.; Forsyth, M. *Electrochim. Acta* **1998**, *43*, 1481.
(14) Forsyth, M.; Meakin, P.; MacFarlane, D. R.; Hill, A. J. *J. Phys.: Condensed Matter* **1995**, *7*, 7601.
(15) Stevens, J. R.; Chung, S. H.; Horoyski, P.; Jeffrey, K. R. *J. of Non-Cryst. Solids* **1994**, *172−174*, 1207.
(16) Sandner, B.; Weinkauf, A.; Reiche, A. German Patent Application P198 30 993.7.
(17) Reiche, A.; Weinkauf, A.; Sandner, B.; Rittig, F.; Fleischer, G. *Electrochim. Acta* **2000**, *45*, 1327.
(18) Weinkauf, A. Thesis, Martin-Luther-University Halle-Wittenberg, 1999.
(19) Reiche, A.; Sandner, R.; Weinkauf, A.; Sandner, B.; Fleischer, G.; Rittig, F. *Polymer* **2000**, *41*, 3821.
(20) Schwarzl, F. R. *Polymermechanik*; Springer-Verlag Berlin: Heidelberg, 1990.
(21) LIFSPECFIT 5.1, Lifetime spectrum fit version 5.1, 1992 (Technical University of Helsinki).
(22) Shukla, A.; Peter, M.; Hoffmann, L. *Nucl. Instrum. Methods* **1993**, *335A*, 310. Hoffmann, L.; Shukla, A.; Peter, M.; Barbiellini, B.; Manuel, A. A. *Nucl. Instrum. Methods* **1993**, *335A*, 276.
(23) Dlubek, G.; Hübner, C. H.; Eichler, S. *Nucl. Instrum. Methods* **1998**, *142B*, 191. Dlubek, G.; Eichler, S. *Phys. Stat. Sol.* **1998**, *168(a)*, 333.
(24) Dlubek, G.; Eichler, S.; Hübner, C. H.; Nagel, C. H. *Nucl. Instrum. Methods* **1999,** *149B*, 501.
(25) Kärger, J.; Bär, N.-K.; Heink, W.; Pfeifer, H.; Seiffert, G. *Z. Naturforsch.* **1995**, *50A*, 186.
(26) Heink, W.; Kärger, J.; Seiffert, G.; Fleischer, G.; Rauchfuss, J. *J. Magn. Reson. A* **1995**, *114*, 101.
(27) Kärger, J.; Pfeifer, H.; Heink, W. *Adv. Magn. Reson.* **1988**, *12*, 1.
(28) Fleischer, G.; Fujara, F. *NMR Basic Princ. Prog.* **1994**, *30*, 161.
(29) Reisinger, T. J. G.; Scholl, H.-U.; Meyer, W. H. *Chem. Phys. Lett.* **1998**, *283*, 15. Pethrick, R. A. *Prog. Polym. Sci.* **1997**, *22*, 1.
(30) *Structure Reports*; Trotter, J., Ferguson, G., Eds.; 1972; Vol. 38B (II).
(31) Dlubek, G.; Saarinen, K.; Fretwell, H. M. *J. Polym. Sci., Part B: Polym. Phys.* **1998**, *36*, 1513. Dlubek, G.; Stejny, J.; Alam, M. A. *Macromolecules* **1998**, *31*, 4574. Dlubek, R.; Buchhold, C. H.; Hübner, Nakladal, A. *Macromolecules* **1999**, *32*, 2348.

(32) Nakahishi, N. Y.; Jean, C. In *Positron and Positronium Chemistry*; Schrader, D. M., Jean, Y. C., Eds.; Studies in Physical and Theoretical Chemistry, 57; Elsevier Science Publishers: Amsterdam, 1988; p 159.
(33) Dlubek, G.; Fretwell, M. H.; Alam, A. *Phys. Stat. Sol. A* **1998**, *167*, R13.
(34) Tao, S. J. *J. Chem. Phys.* **1972**, *56*, 5499.
(35) Eldrup, E.; Mogensen, M.; Trumpy, G. *J. Chem. Phys.* **1972**, *57*, 495.
(36) *Polymer Handbook*, 3rd ed.; Bandrup, J. E., Immergut, H., Eds.; Wiley: New York, 1989; Vol. VI, p 419.
(37) Unpublished experimental results.
(38) Clericuzio, M.; Parker, W. O.; Soprani, M.; Andrei, M. *Solid State Ionics* **1995**, *82*, 179.
(39) Johansson, A.; Gogoll, A.; Tegenfeldt, J. *Polymer* **1996**, *37*, 1387.
(40) Williamson, M. J.; Southall, J. P.; Hubbard, H. V.; Davies, G. R.; Ward, I. M. *Polymer* **1999**, *40*, 3945.
(41) Shi, J. C.; Vincent, A. *Solid State Ionics* **1993**, *60*, 11.
(42) Reiche, A.; Cramer, T.; Fleischer, G.; Sandner, R.; Sandner, B.; Kremer, F.; Kärger, J. *J. Phys. Chem. B* **1998**, *102 (11)*, 1861.
(43) Appel, M.; Fleischer, G. *Macromolecules* **1993**, *26*, 5520.
(44) Elias, H. G. *Makromoleküle*; Hüthig & Wepf Verlag: Basel, 1990; Band 1, p 878.
(45) Sandner, B.; Tübke, J.; Wartewig, S.; Shaskov, S. *Solid State Ionics* **1996**, *83*, 87.
(46) Reiche, A.; Tübke, J.; Sandner, R.; Werther, A.; Sandner, B.; Fleischer, G. *Electrochim. Acta* **1998**, *43*, 1429.
(47) Fontanella, J. J.; Wintersgill, M. C.; Calame, J. P.; Pursel, F. P.; Figueroa, D. R.; Andeen, C. G. *Solid State Ionics* **1983**, *9 & 10*, 1139.
(48) Stallworth, P. E.; Fontanella, J. J.; Wintersgill, M. C.; Scheidler, C. D.; Immel, J. J.; Greenbaum, S. G.; Gozdz, A. S. Proceedings of the 9th International Conference on Lithium Batteries, Edinburgh, 1998.
(49) Edmondson, C. E.; Wintersgill, M. C.; Fontanella, J. J.; Gerace, F.; Scrosati, B.; Greenbaum, S. G. *Solid State Ionics* **1996**, *85*, 173.
(50) Duclot, M.; Alloin, F.; Brylev, O.; Sanchez, J. Y.; Souquet, J. L. Proceedings of the 12th International Conference on Solid State Ionics, Thessaloniki, 1999.
(51) Furtado, C. A.; Silva, G. G.; Machado, J. C.; Pimenta, M. A.; Silva, R. A. *J. Phys. Chem. B* **1999**, *103*, 7102.
(52) Wang, C. L.; Hirade, T. F.; Maurer, H.; Eldrup, M.; Pedersen, N. J. *J. Chem. Phys.* **1998**, *108*, 4654.